

Explosive Nucleosynthesis in Axisymmetrically Deformed Type II Supernovae

Shigehiro Nagataki¹, Masa-aki Hashimoto², Katsuhiko Sato^{1,3}, and Shoichi Yamada^{1,4}

¹Department of Physics, School of Science, the University of Tokyo, 7-3-1 Hongo, Bunkyo, Tokyo 113, Japan

²Department of Physics, Faculty of Science, Kyusyu University, Ropponmatsu, Fukuoka 810, Japan

³Research Center for the Early Universe, School of Science, the University of Tokyo, 7-3-1 Hongo, Bunkyo, Tokyo 113, Japan

⁴Max-Planck-Institute für Physik und Astrophysik Karl-Schwarzschild Strasse 1, D-8046, Garching bei München, Germany

Received _____; accepted _____

ABSTRACT

Explosive nucleosynthesis under the axisymmetric explosion in Type II supernova has been performed by means of two dimensional hydrodynamical calculations. We have compared the results with the observations of SN 1987A. Our chief findings are as follows: (1) ^{44}Ti is synthesized so much as to explain the tail of the bolometric light curve of SN 1987A. We think this is because the alpha-rich freezeout takes place more actively under the axisymmetric explosion. (2) ^{57}Ni and ^{58}Ni tend to be overproduced compared with the observations. However, this tendency relies strongly on the progenitor's model.

We have also compared the abundance of each element in the mass number range $A = 16 - 73$ with the solar values. We have found three outstanding features. (1) For the nuclei in the range $A = 16 - 40$, their abundances are insensitive to the initial form of the shock wave. This insensitivity is favored since the spherical calculations thus far can explain the solar system abundances in this mass range. (2) There is an enhancement around $A=45$ in the axisymmetric explosion compared with the spherical explosion fairly well. In particular, ^{44}Ca , which is underproduced in the present spherical calculations, is enhanced significantly. (3) In addition, there is an enhancement around $A=65$. This tendency does not rely on the form of the mass cut but of the initial shock wave. This enhancement may be the problem of the overproduction in this mass range, although this effect would be relatively small since Type I supernovae are chiefly responsible for this mass number range.

Subject headings: supernovae: general — supernovae: individual (SN 1987A) — nucleosynthesis

1. Introduction

Supernovae play an important role in ejecting heavy elements produced in massive stars (e.g., Woosley & Weaver 1995 and references therein). It is important to determine the composition of ejected gas as a function of stellar mass since it is basic data for the chemical evolution of galaxies. In this paper, we discuss Type II supernovae, which are regarded as the death of a massive star whose mass exceeds 8 times the solar mass (M_{\odot}) (e.g., Hashimoto 1995).

The mechanism of Type II supernovae has been understood as follows (e.g., Bethe 1990): when the mass of the iron core of the progenitor exceeds the Chandrasekhar mass, the star begins to collapse. The collapse continues until the central density of the collapsing core reaches about 1.5-2 times the nuclear matter density ($\rho = 2.7 \times 10^{14} \text{g cm}^{-3}$), beyond which matter becomes too stiff to be compressed further. A shock wave then forms, propagates outward. At first, the shock wave is not so strong and stall in the Fe core. However, by the neutrino heating, the shock wave is revived, begins to propagate outward again, and finally produces the supernova explosion. This phenomenon is called as delayed explosion, which is the most promising theory for the mechanism of type II supernova explosions.

When the shock wave passes Si- rich and O- rich layers, the temperature becomes high enough to cause many nuclear reactions. This phenomenon is called the explosive nucleosynthesis in Type II supernovae. Many calculations have so far been performed on explosive nucleosynthesis in supernovae (e.g., Woosley & Weaver 1986; Hashimoto, Nomoto, & Shigeyama 1989; Thielemann, Hashimoto, & Nomoto 1990; Hashimoto 1995, Woosley & Weaver 1995).

It is SN 1987A in the Large Magellanic Cloud that has provided the most precise data to test the validity of such calculations. For example, the bolometric luminosity began to increase in a few weeks after the explosion (Catchpole et al 1987; Hamuy et al. 1987), which is attributed to the decay of the radioactive nucleus ^{56}Ni . ^{56}Ni is synthesized during the explosion, and the mass is estimated to be $0.07 - 0.076M_{\odot}$ on the basis of the luminosity study (Shigeyama, Nomoto, & Hashimoto 1988; Woosley & Weaver 1988). ^{57}Ni and ^{44}Ti are also thought to be important nuclei to explain the bolometric light curve. Since the half lives of these nuclei are longer than that of ^{56}Co , their decays are thought to be responsible for the tail of the light curve. In fact, the observed bolometric light curve's decline rate is slowed down since ~ 900 days after explosion (Suntzeff et al. 1991). The ratio of ^{57}Ni to ^{56}Ni is estimated from the X-ray light curve to be 1.5 ± 0.5 times the solar $^{57}\text{Fe}/^{56}\text{Fe}$ ratio (Kurfess et al. 1992). The ratio $^{44}\text{Ti}/^{56}\text{Ni}$ is also estimated and must be larger than 1.8 times the solar $^{44}\text{Ca}/^{56}\text{Fe}$ ratio if the contribution from the pulsar is negligible (Kumagai et al. 1993). There is other important nucleus whose amount is estimated by the observation of SN 1987A. That nucleus is ^{58}Ni , which is produced at the innermost region of the ejecta and gives very important information about the mass cut. From the spectroscopic observation of SN 1987A, the ratio $\langle ^{58}\text{Ni}/^{56}\text{Ni} \rangle \equiv [X(^{58}\text{Ni})/X(^{56}\text{Ni})]/[X(^{58}\text{Ni})/X(^{56}\text{Fe})]_{\odot}$ should be 0.7-1.0 (Rank et al. 1988).

Numerical calculations can reproduce the amount of ^{56}Ni , the ratio of ^{57}Ni to ^{56}Ni , and the ratio of ^{58}Ni to ^{56}Ni (Hashimoto, Nomoto, & Shigeyama 1989). However, the ratio of ^{44}Ti to ^{56}Ni has never been reproduced. It is reported that ^{44}Ti cannot be produced enough to explain the tail of the light curve in wide parameter range (Woosley & Hoffman 1991). Pulsar is another candidate that can explain the light curve. If the energy supply by the pulsar dominates, the light curve will be flat. However, such flatness has not been observed yet. The effect of long recombination and cooling time scales of the remnant is also considered for the explanation (Fransson & Kozma 1993). However, they admit that

their results depend on the model of the progenitor and more careful calculation must be needed for the quantitative estimates. In the present circumstances, the explanation of the bolometric light curve is still open to argument.

There is another touchstone of the numerical simulations. It is the solar system abundances. The appropriate combination of the contribution from Type I and Type II supernova can reproduce the solar system abundance ratios within a factor of 2 for typical species (Hashimoto 1995). However, there are some problems. For example, ^{35}Cl , ^{39}K , and ^{44}Ca are synthesised only about one tenth of the solar value. On the other hand, ^{58}Ni is produced about three times.

Are there any effects which can solve the problems mentioned above, that is, ^{44}Ti problem in SN 1987A and reproduction of the solar system abundance ? We suggest the effect of asymmetric (in particular, axisymmetric) explosion will change the present circumstances. All calculations about nucleosynthesis have been done on the assumption that the explosion is spherically symmetric. However, there are some reasons we should take account of the asymmetry in supernova explosion. Among them is a well-known fact that most massive stars are rapid rotators (Tassoul 1978). Since stars are rotating in reality, the effect of rotation should be investigated in numerical simulations of a collapse-driven supernova. Thus far, several simulations have been done by a few groups in order to study rotating core collapse (Müller, Rozyczka, & Hillebrandt 1980; Tohline, Schombert, & Boss 1980; Müller & Hillebrandt 1981; Bodenheimer & Woosley 1983; Symbalisty 1984; Mönchmeyer & Müller 1989; Finn & Evans 1990; and Yamada & Sato 1994). As a result, some numerical simulations of a collapse-driven supernova suggest the possibility of axisymmetric explosion if the effect of a stellar magnetic field and/or stellar rotation is taken into consideration. There is also possibility that the axisymmetrically modified neutrino radiation from a rotating proto-neutron star causes asymmetric explosion

(Shimizu, Yamada, & Sato 1994). We note these effects mentioned above tend to cause axisymmetric explosion. Furthermore, many observations of SN 1987A suggest the asymmetry of the explosion. The clearest is the speckle images of the expanding envelope with high angular resolution (Papaliolis et al. 1989), where an oblate shape with an axis ratio of $\sim 1.2 - 1.5$ was shown. Similar results were also obtained from the measurement of the linear polarization of the scattered light from the envelope (Cropper et al. 1988). If the envelope is spherically symmetric, there is no net linear polarization induced by scattering. Assuming again that the shape of the scattering surface is an oblate or prolate spheroid, one finds that the observed linear polarization corresponds to an axis ratio of ~ 1.2 .

Because of the reason mentioned above, it is important to investigate the effect of axisymmetric explosion on explosive nucleosynthesis. In the present paper, we calculate the explosive nucleosynthesis for a $20M_{\odot}$ star under the axisymmetric explosion and investigate if the difficulties mentioned above are improved by its effect.

We show our method of calculation for the explosive nucleosynthesis in section 2. Results are presented in section 3. Summary and discussion are given in section 4.

2. Model and Calculations

2.1. Hydrodynamics

We performed 2-dimensional hydrodynamical calculations. The calculated region corresponds to a quarter part of the meridian plane under the assumption of axisymmetry and equatorial symmetry. The number of meshes is 300×10 (300 in the radial direction, and 10 in the angular direction). The inner and outer most radius are set to be 10^8 cm and 2×10^{10} cm, respectively. We use the Roe method for the calculation (Roe 1981; Yamada &

Sato 1994). The basic equations are as follows:

$$\begin{aligned}
 \partial_t \rho &= -\frac{1}{r^2} \partial_r (\rho u_r r^2) - \frac{1}{r \sin \theta} \partial_\theta (\rho u_\theta \sin \theta), \\
 \partial_t (\rho u_r) &= -\frac{1}{r^2} \partial_r (\rho u_r^2 r^2) - \frac{1}{r \sin \theta} \partial_\theta (\rho u_r u_\theta \sin \theta) \\
 &\quad - \partial_r P + \frac{\rho u_\theta^2}{r}, \\
 \partial_t (\rho u_\theta) &= -\frac{1}{r^2} \partial_r (\rho u_\theta u_r r^2) - \frac{1}{r \sin \theta} \partial_\theta (\rho u_\theta^2 \sin \theta) \\
 &\quad - \frac{1}{r} \partial_\theta P - \frac{\rho u_\theta u_r}{r}, \\
 \partial_t E &= -\frac{1}{r^2} \partial_r [(E + P) u_r r^2] \\
 &\quad - \frac{1}{\sin \theta} \partial_\theta [(E + P) u_\theta \sin \theta]
 \end{aligned}$$

where ρ , P , and E are the mass density, pressure, total energy density per unit volume and u_r and u_θ are velocities of a fluid in r and θ direction, respectively. The first equation is the continuity equation, the second and third are the Euler equations and the fourth is the equation of the energy conservation. We use the equation of state:

$$P = \frac{1}{3} a T^4 + \frac{\rho k_B T}{A_\mu m_u}$$

where a , k_B , A_μ and m_u are the radiation constant, Boltzmann constant, the mean atomic weight, and the atomic mass unit, respectively.

In this paper, we assume the system is adiabatic after the passage of the shock wave, because the entropy produced during the explosive nucleosynthesis is much smaller than that generated by the shock wave. As a result, the entropy per nucleon is conserved.

2.2. Post-processing

In order to calculate the change of the chemical composition of the star, we use a test particle approximation. $(10(r) \times 10(\theta))$ and $(40(r) \times 10(\theta))$ particles are scattered in the Si-rich and O-rich layers, respectively, with the increasing interval in the radial directions and same interval in the angular ones in each layer. This is because explosive nucleosynthesis can occur mainly in the inner region where the temperature reach high enough to cause nuclear reactions. On the other hand, little change occurs in the outer region and we do not need to scatter many particles in the outer region.

We preserve the time evolution of density and temperature along each trajectory of test particles. It is assumed that test particles are at rest at first and move with the local velocity at their positions after the passage of a shock wave. Thus we can calculate each particle's path by integrating $\frac{\partial \vec{x}}{\partial t} = \vec{v}(t, \vec{x})$, where the local velocity $\vec{v}(t, \vec{x})$ is given from the hydrodynamical calculations mentioned above. The density and the temperature of a test particle at each time are determined by interpolation in the Eulerian mesh the particle is in at the moment. Nucleosynthesis calculations are done separately for each trajectory of test particles using a nuclear reaction network explained below (after the hydrodynamical simulations). In calculating the total yields of elements we assume that each test particle has its own mass which is determined from the initial distribution of the test particles so that their sum becomes the mass of the Si-rich and O-rich layers, and also assume that the nucleosynthesis occurs uniformly in each mass element. In this way, the total chemical composition can be calculated by summing the final chemical composition of each mass element weighted by its mass.

It is noted that the above assumption is valid when the typical size of a test particle calculated from its mass and density is smaller than the temperature scale height at its position. It is also necessary that the shear of the flow is not very large in the mass element. In this calculation we assumed that the initial velocity of the matter is radial

behind the shock wave (see §2.4) and the time scale of the explosive nucleosynthesis is small (~ 1 sec), we think this assumption is not so bad. Regardless, this is only the first step of the estimation of chemical abundances in an axisymmetric supernova explosion, and improvement in resolution of mesh and test particles is now underway.

2.3. Nuclear reaction network

We have calculated the explosive nucleosynthesis using the time evolution of (ρ, T) discussed in §2.2. Since the system is not in chemical equilibrium, we must calculate the change of the chemical composition with the use of the nuclear reaction network. It contains 242 species (see Figure 1, Hashimoto, Nomoto, & Shigeyama 1989). The basic equations for the abundance changes are

$$\begin{aligned} \partial_t y_i &= \alpha_{ijkl} y_j y_k y_l + \beta_{ijk} y_j y_k + \gamma_{ij} y_j, \\ y_i &= n_i / (\rho N_A), \end{aligned}$$

where n_i is the number density of i -th nucleus i and N_A is Avogadro's number. Reaction rates are defined by α_{ijkl} , β_{ijk} , and γ_{ij} which have dimensions of sec^{-1} . The first term of the right hand side represents 3-body reactions such as the triple-alpha process, the second is for 2-body, and the third is for 1-body such as the photo-disintegration or β decay. We integrate this system of coupled differential equations by an implicit method (Hashimoto, Hanawa, & Sugimoto 1983). To construct a large network relevant for the calculation of the explosive nucleosynthesis, data of reaction rates were used from various sources (e.g., Hashimoto & Arai 1985).

EDITOR: PLACE FIGURE 1 HERE.

2.4. Initial conditions

The progenitor of SN 1987A, Sk-69°202, is thought to have had the mass $\sim 20M_{\odot}$ in the main-sequence stage (Shigeyama, Nomoto, & Hashimoto 1988; Woosley & Weaver 1988) and had $\sim (6\pm 1)M_{\odot}$ helium core (Woosley 1988). In the present paper, the presupernova model which is obtained from the evolution of a helium core of $6 M_{\odot}$ (Nomoto & Hashimoto 1988) is used for the initial density and composition. Table 1 shows the radii of the Fe/Si, Si/O and O/He interfaces in this model.

We will explain the initial shock wave. Since there is still uncertainty as to the mechanism of type II supernova, precise explosive nucleosynthesis calculations have not been performed from the beginning of core collapse. Instead, explosion energy is deposited artificially at the innermost boundary (e.g., Hashimoto 1995). There is another method used by Woosley (“the method of the piston”, see Woosley & Weaver 1995). However, both methods are only approximation and the initial condition has been problem of the explosive nucleosynthesis. In this paper, the method of energy deposition is taken and the explosion energy of 1.0×10^{51} erg is injected to the region from 1.0×10^8 cm to 1.5×10^8 cm (that is, at the Fe/Si interface).

As for the axisymmetric explosion, the initial velocity of matter behind the shock wave is assumed to be radial and proportional to $r \times \frac{1+\alpha \cos(2\theta)}{1+\alpha}$, where r , θ , and α are radius, the zenith angle, and the free parameter which determine the degree of the axisymmetric explosion, respectively. Since the ratio of the velocity in the polar region to that in the equatorial region is $1 : \frac{1-\alpha}{1+\alpha}$, more extreme jet-like shock waves is obtained as the α gets larger. In the present study, we take $\alpha = 0$ for the spherical explosion and $\alpha = \frac{1}{3}$, $\frac{3}{5}$, and $\frac{7}{9}$ (these values mean that the ratios of the velocity are 2:1, 4:1, and 8:1, respectively) for the axisymmetric ones (see Table 2). We assumed that the distribution of thermal energy

is same as the velocity distribution and that total thermal energy is equal to total kinetic energy.

We note that the form of the initial shock wave can not be known directly from both observation and theory. As a result of it, the value of α can not be known *a priori*. However, it is reported that there is a possibility for a shock wave to be jet-like if the proper angular momentum of the progenitor is assumed (Yamada & Sato 1994). Because of this reason, we think our formulation of the initial shock wave is not so unreasonable. At least, there is a possibility for the shock wave to be axisymmetric as we have assumed. Moreover, the value of α to be desired in SN 1987A would be in this range as shown in section 3.

EDITOR: PLACE TABLE 1 HERE.

EDITOR: PLACE TABLE 2 HERE.

3. Results

3.1. Reproduction of observational data of SN 1987A

3.1.1. Mass cut

In type II supernova, there is boundary that separates ejecta and central compact object. This boundary is called as the mass cut. Strictly speaking, the position of the mass cut should be determined by hydrodynamical calculation including gravity, that is,

the matter which has positive total energy (sum of the kinetic, thermal, and gravitational energy) can escape and that which has negative energy falls back to central compact object. However, it is very difficult to determine the position of the mass cut hydrodynamically since it is sensitive not only to the explosion mechanism, but also to the presupernova structure, stellar mass, and metallicity. In fact, it is reported that total amount of ^{56}Ni can not be reproduced by the piston method, which determines the mass cut hydrodynamically (Woosley & Weaver 1995).

There is another way to determine the position of the mass cut. Among many observational data of SN 1987A, the total amount of ^{56}Ni in the ejecta is one of the most reliable one. For that reason, the position of the mass cut can be determined so as to contain $\sim 0.07M_{\odot}$ ^{56}Ni in the ejecta (Hashimoto 1995). We took the same way in this paper. However, this method is simple only for spherical calculations. We must extend this method for multi-dimensional calculations as follows: we assume that the larger total energy (internal energy plus kinetic energy) a test particle has, the more favorably it is ejected (Shimizu, Yamada, & Sato 1993). We first calculate the total energy of each test particle at the final stage of our calculations (~ 10 sec) and then add up the mass of ^{56}Ni in a descending order of the total energy until the summed mass reaches $0.07M_{\odot}$. The rest of ^{56}Ni is assumed to fall back to the central compact object even if it has a positive energy at that time. We show the position of the mass cut for each model in Figures 2 and 3. We note the dots, which show test particles which will be ejected, are plotted for their initial positions. In this way, the position of the mass cut is easily determined. The tendency that more matter around the polar axis is ejected is consistent with the initial form of the shock wave. We refer to this mass cut as A7. To see the dependence of our analysis on the position of the mass cut, we take another mass cut for comparison. This mass cut is set to be spherical and determined so as to contain $0.07M_{\odot}$ ^{56}Ni in the ejecta. We refer to this mass cut as S7.

EDITOR: PLACE FIGURE 2 HERE.

EDITOR: PLACE FIGURE 3 HERE.

3.1.2. Comparison with SN 1987A

We show the ratios $\langle {}^{44}\text{Ti}/{}^{56}\text{Ni} \rangle$, $\langle {}^{57}\text{Ni}/{}^{56}\text{Ni} \rangle$, and $\langle {}^{58}\text{Ni}/{}^{56}\text{Ni} \rangle$. These quantities are defined as below:

$$\begin{aligned} \langle {}^{44}\text{Ti}/{}^{56}\text{Ni} \rangle &\equiv [X({}^{44}\text{Ti})/X({}^{56}\text{Ni})]/[X({}^{44}\text{Ca})/X({}^{56}\text{Fe})]_{\odot} \\ \langle {}^{57}\text{Ni}/{}^{56}\text{Ni} \rangle &\equiv [X({}^{57}\text{Ni})/X({}^{56}\text{Ni})]/[X({}^{57}\text{Fe})/X({}^{56}\text{Fe})]_{\odot} \\ \langle {}^{58}\text{Ni}/{}^{56}\text{Ni} \rangle &\equiv [X({}^{58}\text{Ni})/X({}^{56}\text{Ni})]/[X({}^{58}\text{Ni})/X({}^{56}\text{Fe})]_{\odot} \end{aligned}$$

where X denotes mass fraction. At first, there is a fact to which we must pay attention. It is reported that this $6 M_{\odot}$ model is neutron-rich and the value of Y_e for $M > 1.607 M_{\odot}$ ($=0.494$) is artificially changed to that of $M > 1.637 M_{\odot}$ ($=0.499$) to suppress the overproduction of neutron-rich nuclei (Hashimoto 1995). This means the range of convective mixing in the presupernova model is artificially changed. Anyway, at first, we also modify the $6 M_{\odot}$ model in the same way. The result is summarised in Table 3 (Case A in the Table). We can see clearly that ${}^{44}\text{Ti}$ is more produced as the degree of the axisymmetric explosion gets larger. It is also noted that ${}^{44}\text{Ti}$ is produced so much in the axisymmetric explosion as to explain the tail of the bolometric light curve of SN 1987A. Since ${}^{44}\text{Ti}$ is synthesised through the alpha-rich freezeout, high entropy is needed for the synthesis of

this nucleus. Since the matter becomes radiation dominated after the passage of the shock wave, the entropy per baryon can be written approximately as below:

$$S_\gamma = \frac{16\sigma}{3k_B c} m_u \frac{T^3}{\rho N_A}$$

where σ , k_B , c , m_u , T , ρ , and N_A are Stefan-Boltzmann constant, Boltzmann constant, speed of light, atomic mass unit, temperature, density, and Avogadro constant, respectively. The entropy is normalized in unit of k_B . We show distributions of the entropy per nucleon for S1 and A3 models in Figure 4. We note the contours are drawn for the initial positions of the test particles. It is clear from Figure 4 that higher entropy is achieved in the polar region for the axisymmetric explosion. We will explain this tendency. The relation between energy density and temperature behind the shock wave can be written approximately as below:

$$E[\text{erg}/\text{cm}^3] = aT^4$$

where a is radiation constant. As more energy is deposited initially in the polar region, higher temperature is achieved. As a result of it, higher entropy is achieved in the polar region than the equatorial region. We show in Figure 5 the contour of ^{44}Ti and ^4He in A3 model. ^{44}Ti is produced much in the polar region together with ^4He , as expected.

EDITOR: PLACE FIGURE 4 HERE.

EDITOR: PLACE FIGURE 5 HERE.

On the other side, ^{57}Ni and ^{58}Ni are overproduced and inconsistent with the observations in the axisymmetric explosion. This is because the ejecta contains the neutron-rich matter in the polar region for the axisymmetric explosion cases (see Fig 2

and 3). We note that even if the mass cut is set to be spherical, the ejecta contains more neutron-rich matter in the axisymmetric case. This is because the mass cut tends to be smaller in axisymmetric explosion since ^{56}Ni is less produced (see the mass cut of S7 in Table 3). To see the effect of neutron-rich matter, we perform the same calculations for the modified $6 M_{\odot}$ model, in which the value of Y_e for $M > 1.5M_{\odot}$ is artificially changed to that of $M > 1.637M_{\odot}$. The results are summarised in Table 3 (Case B in the Table). We can see the amount of ^{44}Ti is still much enough to explain the light curve, with the amount of ^{57}Ni and ^{58}Ni consistent with the observations. This means that the uncertainty of the presupernova model have a great influence on the chemical composition of the ejecta.

We will give an additional comment on the mass cut and the mass of the central compact object. There is a tendency that as the degree of the axisymmetric explosion gets larger, the mass of the central compact object also becomes larger if the mass cut is set to be A7 (see Table 3). In particular, there is a possibility that the mass of the central object is large enough to cause gravitational collapse and forms black hole, instead of neutron star. If the pulsar will be not found in SN 1987A, it may be worth considering this effect seriously.

EDITOR: PLACE TABLE 3 HERE.

3.2. Comparison with the solar system abundances

Next, we calculate the total amount of heavy elements in the range $A = 16 - 73$ and compare them with solar system abundances. We note that the informations about initial mass function (IMF), chemical composition of ejecta for each mass range of the progenitor,

and the ratio of Type I and type II supernova are necessary when the reproduction of solar system abundances is attained. In this paper, we can only make a suggestion for the degree of impact of axisymmetric explosion on the reproduction of solar system abundances, because we have calculated only with $6 M_{\odot}$ model. The calculations of explosive nucleosynthesis for wide range of progenitor’s mass are now underway.

We will comment on this analysis. At first, all unstable nuclei produced in the calculation are assumed to decay to the corresponding stable nuclei when compared with the solar values. Secondary, two forms of the mass cut, which are mentioned above, are used in this analysis to see its influence on the result.

Figures 6 and 7 show the results for three models, that is, the S1, A1, and A3 cases for the mass cut of A7. Figure 6 shows the comparison of the composition for $A = 16 - 73$ normalized by the S1 case. Open circles denote the A1/S1 and dots denote the A3/S1. Figure 7 illustrates the comparison of the abundances of ejected nuclei with the solar values (normalized at ^{16}O). It is evident from the Figure 6 that the amount of nuclei in the range $A = 16 - 40$ is almost same among three models and there are two peaks around $A = 45$ and $A = 65$. We will comment on these three outstanding feature. At first, it is the important result that the amount of nuclei is hardly changes in the range $A = 16 - 40$, since spherical calculations can reproduce well the solar system abundances in this range (Hashimoto 1995). Secondary, the enhanced nuclei near $A = 45$ are ^{44}Ca , ^{47}Ti , ^{48}Ti , and ^{52}Cr , which are synthesized by the alpha-rich freezeout like ^{44}Ti in subsection 3.1.2. We can say that this enhancement is an additional evidence for the more active alpha-rich freezeout under the axisymmetric explosion. Thirdly, the peak around $A = 65$ is thought to be made by the strong shock in the polar region in the axisymmetric explosion, which can cause nuclear reaction against the coulomb repulsion. Figure 8 is same as Figure 6 but for the mass cut of S7. The peak around $A=65$ still exists and this suggests the feature of overproduction of

heavy elements around $A=65$ is fatal one for the axisymmetric explosion.

We will pay attention to each nuclei individually. As mentioned in section 1, it is reported that ^{35}Cl , ^{39}K , ^{44}Ca are underproduced and ^{58}Ni is overproduced in spherical calculations to date. The amounts of ^{35}Cl and ^{39}K produced by the asymmetric explosion are almost the same as those by the spherical explosion. However, ^{44}Ca is produced more and may save the less production of it in spherical calculation. For ^{58}Ni , it is very sensitive to the Y_e of the progenitor and position of the mass cut. However, we can say that neutronization should be also suppressed in the axisymmetric explosion as seen in section 3.1 to be consistent with the observation.

EDITOR: PLACE FIGURE 6 HERE.

EDITOR: PLACE FIGURE 7 HERE.

EDITOR: PLACE FIGURE 8 HERE.

4. Summary and Discussion

We have calculated the explosive nucleosynthesis in the supernova of $6M_{\odot}$ helium core on the assumption that the explosion is axisymmetric. We inspected the effect of axisymmetric explosion by comparing the results with the observation of SN 1987A and solar system abundances.

As for SN 1987A, it is shown that ^{44}Ti is produced in the axisymmetric explosion so much as to explain the tail of the light curve. To put it differently, the degree of the axisymmetric explosion must be that in our models at least to explain that observation. Although our forms of the initial shock wave are only assumption, our results suggest the lower constraint on the degree of the axisymmetric explosion by the amount of ^{44}Ti . We note that some our results strains the limits set on $\frac{^{44}\text{Ti}}{^{56}\text{Ni}}$ under the spherical explosion (Woosley & Hoffman 1991). We think this is because the localized energy in the polar region introduce high entropy and produces much ^{44}Ti there. It is difficult to estimate precisely its amount by the bolometric light curve because of the presence of the bright optical surroundings and the freeze out effect (Fransson & Kozma 1993). However, this amount would be identified from observations by X-ray and γ -ray satellites in future. Therefore, the observation of it may reveal the effects of an axisymmetric explosion.

Moreover, it is reported that the estimated mass of ^{44}Ti by the observation of Cas A shows $(1.4\pm 0.4)-(3.2\pm 0.8)\times 10^{-4}M_{\odot}$ (Iyudin et al. 1994). Although its abundance is still controversial, this value is more than that which is predicted by spherical calculation (Timmes et al 1996). Since the form of the Cas A remnant is far from spherical, it may support our results.

There will be nothing to be complained of if the amount of other nuclei such as ^{57}Ni and ^{58}Ni are consistent with observations. However, in the present study, the amount of them tend to be overproduced in the axisymmetric explosion. It is noted that the $6M_{\odot}$ helium core is in itself too neutron-rich in Si layer and the value of Y_e needs to be modified to explain the observed ^{58}Ni even in the spherical explosion (Hashimoto 1995). We also showed in this paper that if the value of Y_e in Si layer is modified the amount of ^{57}Ni and ^{58}Ni can be in the range of the observation with the amount of ^{44}Ti hardly changed. It will be necessary to perform our calculation with various presupernova model to see the

dependence of our results on the progenitor’s model, in particular, Y_e distribution.

We also compared the results with solar system abundances. There are three outstanding features in the axisymmetric explosion. One is that the amount of nuclei in the range $A = 16 - 40$ is hardly changed by the form of the initial shock wave. The others are that there are two peaks around $A = 45$ and $A = 65$. The insensitivity of these nuclei is good for axisymmetric explosions because of the fact that the spherical calculations thus far can explain the solar system abundances well in this range (for the spherical case, see Hashimoto 1995). However, we cannot also solve the problem of the underproduction of ^{35}Cl and ^{39}K . We note ^{44}Ca , which is mainly synthesised through the decay of ^{44}Ti , is produced more in the axisymmetric explosion. This means the axisymmetry of explosion has a positive effect on explaining the solar values of this nucleus. On the other hand, the effect of the peak around $A = 65$ may be relatively small since Type I supernovae are chiefly responsible for this mass number range (e.g., Hashimoto 1995). This means, fortunately, the problem of overproduction of heavy elements in this range may not occur. We are now calculating explosive nucleosynthesis for wide range of progenitor’s mass and will report on this influence in the near future. We will give an additional comment. The more production of ^{44}Ca means the more active alpha-rich freezeout, that is, more helium is remained because of high entropy per baryon. We should note that ^4He produced in this region may have an effect on the production of ^7Li through the neutrino process. In addition, the production of ^7Li becomes more efficient if axisymmetric radiation of neutrinos (Shimizu, Yamada, & Sato 1994) causes the explosion axisymmetric.

We will consider the reliability of our calculations. As for the mesh resolution, 10 angular zones may seem coarse. However, in the calculation of explosive nucleosynthesis, convection will not play an important role and we think high mesh resolution is not needed. We are doing more precise calculation using a supercomputer now. We will estimate the

dependence of results on mesh resolution in future. In addition, we should explore the sensitivity of results to the initial condition, such as total explosion energy, the ratio of initial thermal energy to kinetic energy, and initial radius of the shock wave. This is because with either method for the initial shock condition, that is, the method of depositing energy and of the piston, the peak temperatures are incorrect in the early history of the shock (Aufderheide et al. 1991). In the present circumstances, there is no self-consistent way to produce initial shock wave and the only thing we can do would be to calculate with various initial conditions. Finally, we comment on the dimension of the simulations. All the simulations presented here are performed in two dimensions since three dimensional computations require much more computer time and memory. Two dimensional calculation may limit some flow modes which are allowed in three dimensional simulations. As a result of it, the entropy per baryon may be kept higher in the polar region after the passage of the shock wave, which generates much ^{44}Ti in two dimensional calculations. However, we think its influence will be small since equatorial symmetry will be kept approximately in the jet-like explosion and convection will not play an important role in this study. Anyway, we should examine this two dimensional effect in future. We will estimate the influence of these effects mentioned above and confirm the credibility of each calculation.

We have done the calculation of the explosive nucleosynthesis under the axisymmetric explosion for the first time. The feature of axisymmetric explosion may have a lot of attractions in addition to explosive nucleosynthesis. For example, it is shown that a part of ^{56}Ni can be mixed into the outer layer by Rayleigh-Taylor instabilities in the jet-like explosion with smaller perturbations compared with spherical explosion (Yamada & Sato 1991). In addition, the axisymmetric mass cut and jet-like explosion may be advantageous for ejecting r-process matter. The amount of r-process material which is ejected should be very little, and simultaneously, must be ejected. We think the jet-like explosion will be one of the mechanism which can explain such characteristic. Moreover, some effects such as a

rotation of the progenitor may show the axisymmetric explosion and it may be essential feature for presupernova to explode (e.g., Yamada & Sato 1994, Mönchmeyer, Schäfer, Müller, & Kates 1991).

This work is the first step for the explosive nucleosynthesis under the axisymmetric explosion. However, the axisymmetric explosion have a possibility to solve many mysteries of supernova explosion. We will calculate axisymmetric explosive nucleosynthesis systematically for various progenitor models with different masses to reveal the influence of axisymmetric explosions more clearly.

S. N. is grateful to T. Shimizu and Y. Inagaki for a useful discussion. We are also grateful to E. Skillman for his kind review of the manuscript. M. H. would like to thank M. Arnould and M. Rayet for their hospitality during his stay at Université Libre de Bruxelles. We thank S. Woosley for providing us with the details of his progenitor models and for his kind comments on this manuscript. This work has been supported in part by the Grant-in-Aids for Scientific Research from the Ministry of Education, Science, and Culture of Japan (07CE2002, 07640386, and 07304033).

REFERENCES

- Aufderheide M. B., Baron E., and Thielemann F. K. 1991, *ApJ*, 370, 630
- Bethe 1990, *Rev. Mod. Phys.* 62, 801
- Bodenheimer P., Woosley S.E. 1983, *ApJ*, 269, 281
- Catchpole R. et al 1987, *MNRAS*, 229, 15
- Cropper M., Bailey J., McCowage J., Cannon R.D., Couch W.J., Walsh J.R., Strade J.O.,
and Freeman F. 1988, *MNRAS*, 231, 695
- Finn L.S., Evans C.R. 1990, *ApJ*, 351, 588
- Fransson C., and Kozma C. 1993, *ApJ*, 408, L25
- Hamuy M., Suntzeff N.B., Gonzalez R., Martin G. 1987, *A.J.*, 95, 63
- Hashimoto M., Hanawa T., Sugimoto D. 1983, *Publ.Astron.Soc.Japan*, 35, 1
- Hashimoto M., Arai K. 1985, *Phys.Rep.Kumamoto Univ*, 7, 1
- Hashimoto M., Nomoto k., Shigeyama T. 1989, *A&A*, 210, L5
- Hashimoto M. 1995, *Prog. Theor. Phys.*, 94, 663
- Iyudin A.F. et al., 1994, *A&A*, 284, L1
- Iyudin A.F. et al., 1996, in *Proceedings of the 2nd INTEGRAL Workshop “The Transparent Universe”*, St. Malo, France, ESA SP-382, p.37
- Khokhlov, A.M. 1991, *A&A*, 246, 383
- Kumagai S. Shigeyama T., Nomoto K., Hashimoto M., and Itho S. 1993,*A&A*, 273, 153

- Kurfess J. D., Johnson W. N., Kinzer R. L., et al., 1992, *ApJ*, 399, L137
- Mönchmeyer R.M., Müller E. 1989 in NATO ASI Series, Timing Neutron Stars, p.549,
ed.H.Ögelman & E.P.J.van den Heuvel (New York:ASI)
- Mönchmeyer R., Schäfer G., Müller E., Kates R. E. 1991, *A&A*, 246, 417
- Müller E., Rozyczka M., Hillebrandt W. 1980, *A&A*, 81, 288
- Müller E., Hillebrandt W. 1981, *A&A*, 103, 358
- Nomoto K., Hashimoto M. 1988,*Phys. Rep.*, 163, 13
- Papaliolis C., Karouska M., Koechlin L., Nisenson P., Standley C., Heathcote S. 1989,
Nature, 338, 13
- Shigeyama T., Nomoto K., Hashimoto M. 1988, *A&A*, 196, 141
- Shimizu T., Yamada S., Sato K. in *Numerical Simulations in Astrophysics*, eds. Franco J.,
Lizano S., Aguliar L., and Daltabuit E. (Cambridge Univ. Press, Cambridge) p.170
- Shimizu T., Yamada S., Sato K. 1994, *ApJ*, 432, L119
- Suntzeff B., Phillips M., DePoy L., Elias H., and Wlaker R. 1991, *A.J.*, 102, 1118
- Symbalisty E.M.D. 1984, *ApJ*, 285, 729
- TimmesF.X., WoosleyS.E., HartmannD.H., HoffmanR.D. 1996, *ApJ*, 464, 332
- Rank D. M., Pinto P.A., Woosley S.E., et al., 1988, *Nature*, 331, 505
- Roe P.L. 1981, *Journal of Computational Physics*, 43, 357
- Tassoul J.L. 1978, *Theory of Rotating stars* (Princeton: Princeton Univ. Press)
- Thielemann F.-K., Hashimoto M., Nomoto K. 1990, *ApJ*, 349, 222

- Timmes, F.X., Woosley, S.E., and Weaver, T.A. 1995, *ApJS*, 98, 617
- Tohline J.E., Schombert J.M., Boss A.P. 1980 *Space Sci. Rev.*, 27, 555
- Woosley S.E., Weaver T.A. 1986, *ARA&A*, 24, 205
- Woosley S.E. 1988, *ApJ*, 330, 218
- Woosley S.E., Weaver T.A. 1988, *Phys. Rep.*, 163, 79
- Woosley S.E., Hoffman R.D., 1991, *ApJ*, 368, L31
- Woosley S.E., Weaver T.A. 1995, *ApJS*, 101, 181
- Yamada S., Sato K. 1991, *ApJ*, 382, 594
- Yamada S., Sato K. 1994, *ApJ*, 434, 268

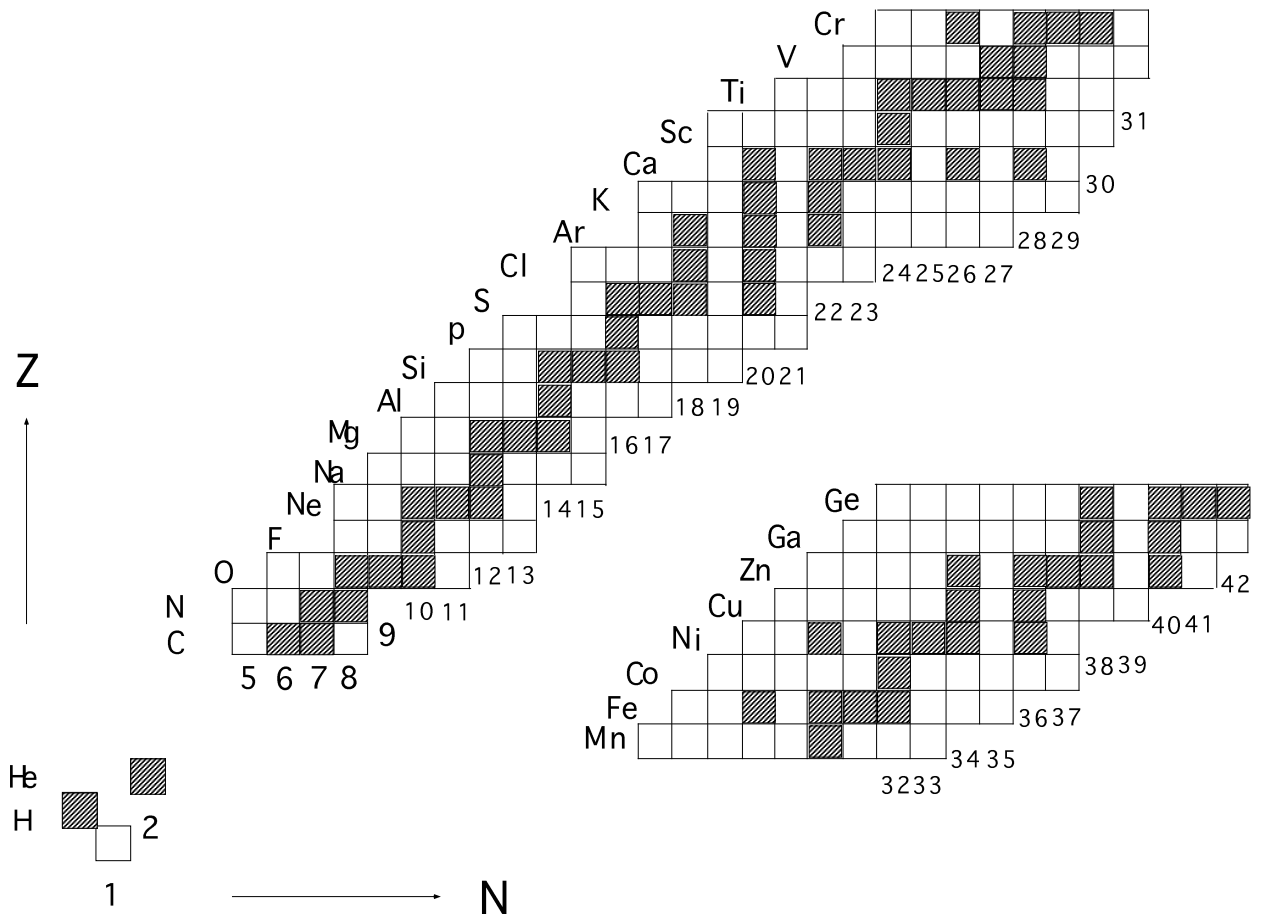


Fig. 1.— Table of nuclei included in our nuclear reaction network. 242 species are included. The gray-colored nuclei denote stable nuclei.

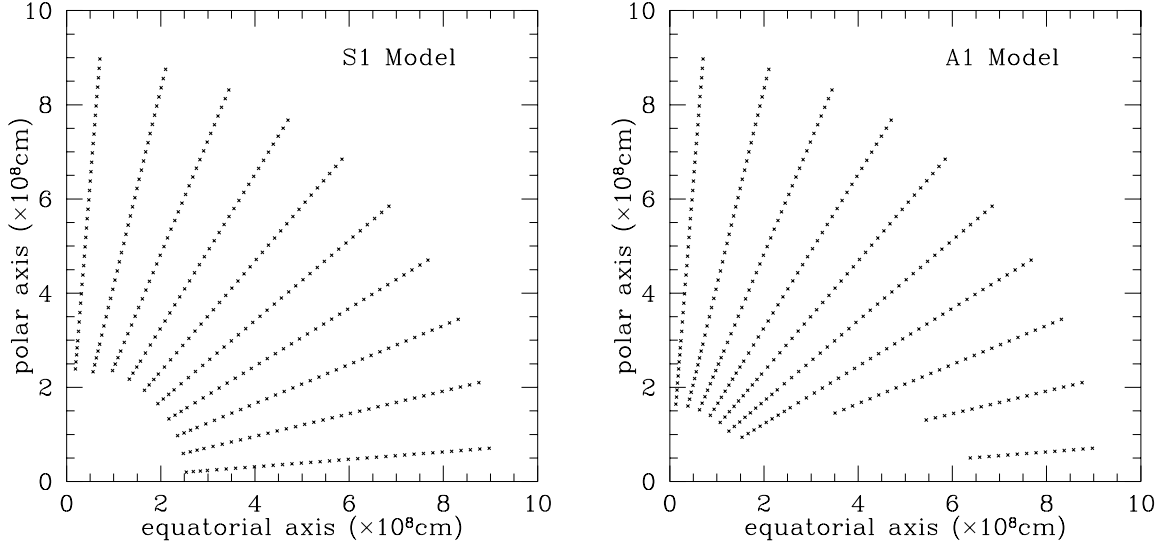


Fig. 2.— Form of the mass cut (A7 model) for S1 case and A1 case. Dots are plotted for the initial positions of the test particles which will be ejected.

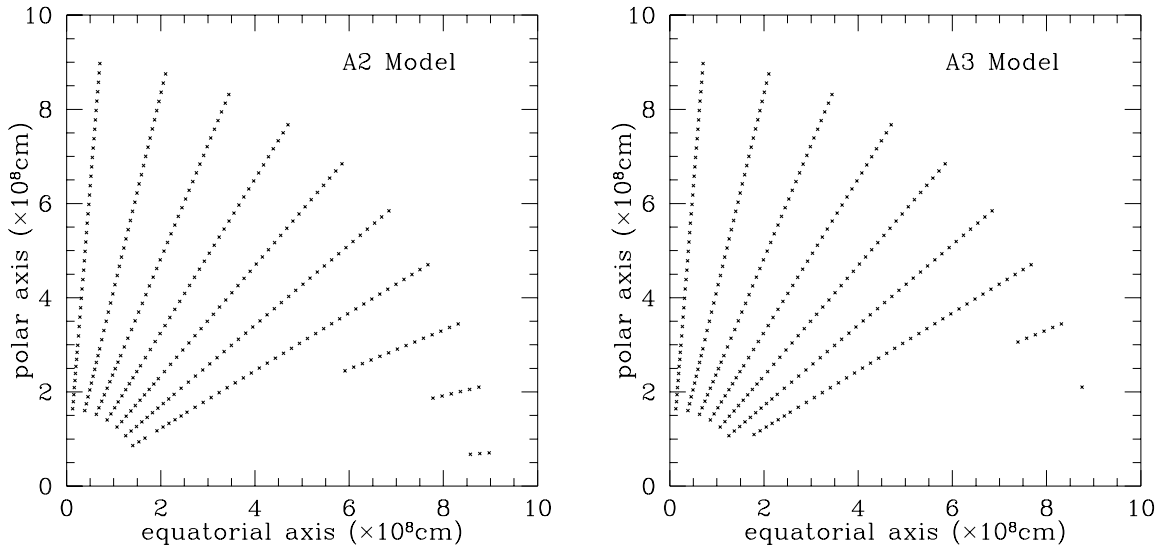


Fig. 3.— Same as Fig.2 but for A2 and A3 case.

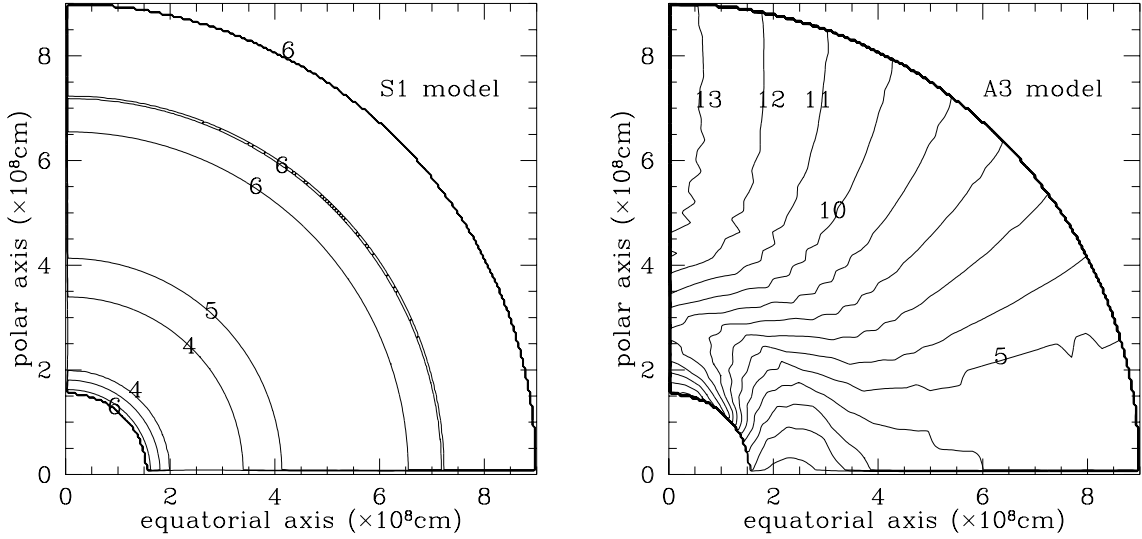


Fig. 4.— Distributions of the entropy for the two cases (left : S1 model, right : A3 model). Entropy is normalized by k_B . Contours are drawn for the initial position of test particles.

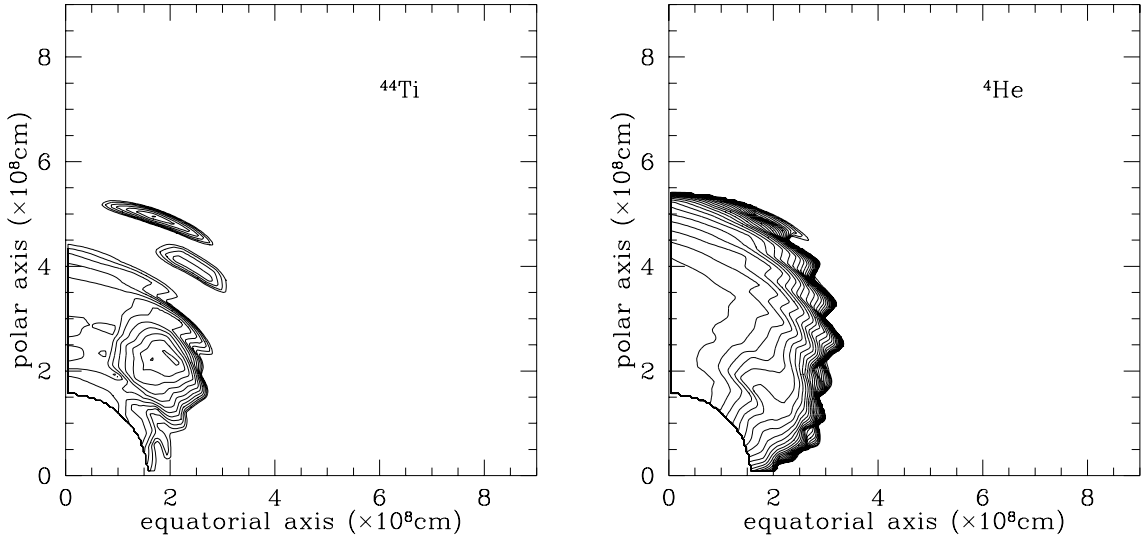


Fig. 5.— Left: Contour of the mass fraction of ^{44}Ti in the A3 case. The maximum value of the mass fraction of ^{44}Ti is 1.3×10^{-2} . Right : Same as left but for ^4He . The maximum value is 4.0×10^{-1} . Contours are drawn for the initial position of test particles.

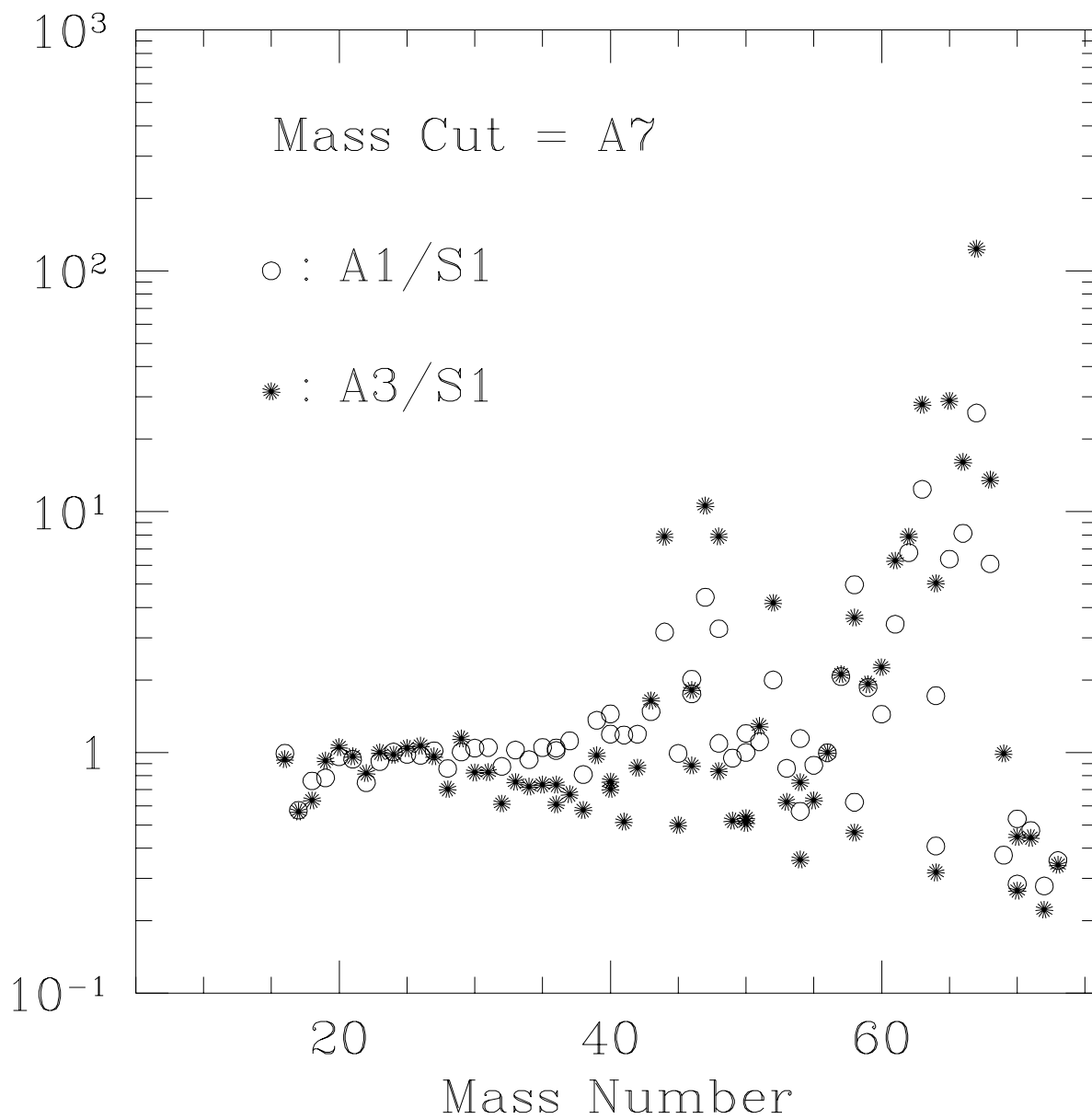


Fig. 6.— Comparison of the composition for the mass number range $A = 16 - 73$ normalized by S1 model. The mass cut is set to be A7. Open circles denote the A1/S1 and dots denote A3/S1. The enhanced nuclei near $A = 45$ are ^{44}Ca , ^{47}Ti , ^{48}Ti , and ^{52}Cr , respectively.

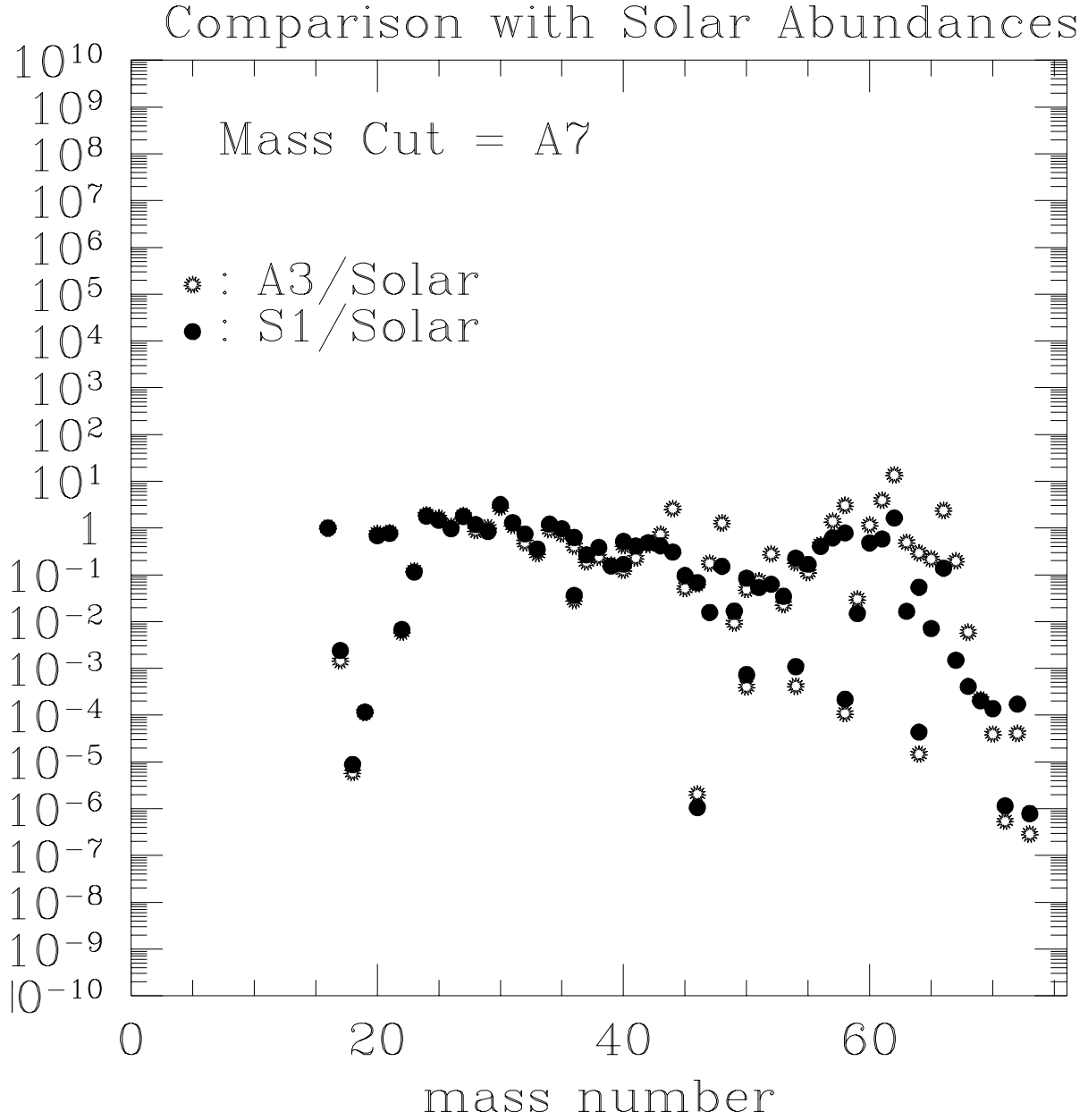


Fig. 7.— Comparison of the abundance of each nucleus with the solar value (normalised to ¹⁶O). Open circles and solid points correspond to S1/solar and A3/solar, respectively.

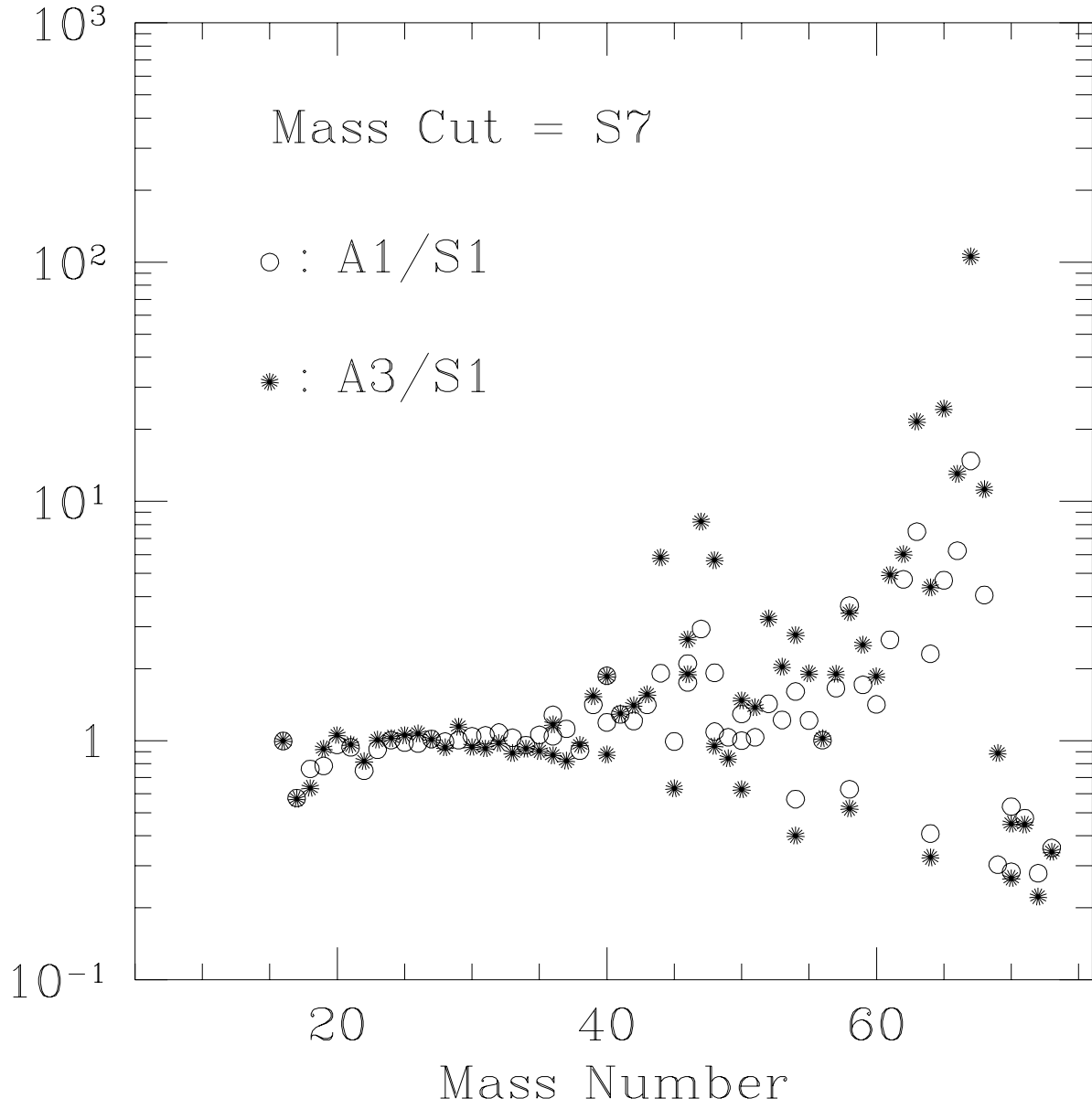


Fig. 8.— Same as Fig.6 but for the mass cut of S7.

Table 1. Radius of the interface for each layer

interface	radius [cm]	radius [M_{\odot}]
Fe/Si	1.5×10^8	1.4
Si/O	3.0×10^8	1.7
O/He	6.3×10^9	3.8

Model	S1	A1	A2	A3
α	0	1/3	3/5	7/9
$V_p:V_e$	1:1	2:1	4:1	8:1

Table 2: Models for the initial shock wave. The first column shows names for each model. Second is the value of α for each model. Third is the ratio of the velocity in the polar region ($\theta = 0^\circ$) to that in the equatorial region ($\theta = 90^\circ$).

Y_e^a	Model	Mass Cut	Mass of NS	$\langle^{44}\text{Ti}/^{56}\text{Ni}\rangle^b$	$\langle^{57}\text{Ni}/^{56}\text{Ni}\rangle^c$	$\langle^{58}\text{Ni}/^{56}\text{Ni}\rangle^d$
Case A	S1	S7	$1.59M_\odot$	0.74	1.5	2.0
Case A	A1	S7	$1.57M_\odot$	1.4	2.5	7.1
Case A	A2	S7	$1.56M_\odot$	2.2	2.8	7.5
Case A	A3	S7	$1.55M_\odot$	4.3	2.8	6.6
Case A	S1	A7	$1.59M_\odot$	0.74	1.5	2.0
Case A	A1	A7	$1.57M_\odot$	2.4	3.2	9.8
Case A	A2	A7	$1.61M_\odot$	3.7	3.3	8.8
Case A	A3	A7	$1.68M_\odot$	6.0	3.2	7.1
Case B	S1	S7	$1.59M_\odot$	0.76	1.5	1.5
Case B	A1	S7	$1.59M_\odot$	1.4	1.7	1.9
Case B	A2	S7	$1.58M_\odot$	1.9	1.7	1.8
Case B	A3	S7	$1.57M_\odot$	4.0	1.8	1.6
Case B	S1	A7	$1.59M_\odot$	0.76	1.5	1.5
Case B	A1	A7	$1.63M_\odot$	2.2	1.8	1.5
Case B	A2	A7	$1.75M_\odot$	3.5	1.8	1.3
Case B	A3	A7	$1.80M_\odot$	6.0	1.8	0.97

Table 3: $\langle^{44}\text{Ti}/^{56}\text{Ni}\rangle$, $\langle^{57}\text{Ni}/^{56}\text{Ni}\rangle$, and $\langle^{58}\text{Ni}/^{56}\text{Ni}\rangle$. The value of Y_e for $M > 1.607M_\odot$ ($=0.494$) is artificially changed to that of $M > 1.637M_\odot$ ($=0.499$) for Case A. Case B is same as Case A but for $M > 1.5M_\odot$. Mass Cut means the form of it and Mass of NS means baryon mass of the central compact object (Neutron Star).

^aThe way Y_e is modified. See Table caption.

^b $\langle^{44}\text{Ti}/^{56}\text{Ni}\rangle \equiv [X(^{44}\text{Ti})/X(^{56}\text{Ni})]/[X(^{44}\text{Ca})/X(^{56}\text{Fe})]_\odot$

^c $\langle^{57}\text{Ni}/^{56}\text{Ni}\rangle \equiv [X(^{57}\text{Ni})/X(^{56}\text{Ni})]/[X(^{57}\text{Fe})/X(^{56}\text{Fe})]_\odot$

^d $\langle^{58}\text{Ni}/^{56}\text{Ni}\rangle \equiv [X(^{58}\text{Ni})/X(^{56}\text{Ni})]/[X(^{58}\text{Ni})/X(^{56}\text{Fe})]_\odot$